

RESEARCH ARTICLE OPEN ACCESS

Effects of Partial Substitution of Ordinary Portland Cement With Stone-Cutting Dust, Limestone, and Natural Pozzolana on Compressive Strength and Microstructure

Nancy Mweni Paul¹  | Jackson Wachira Muthengia¹  | Genson Murithi¹  | Esther Wanja Nthiga²  |
Joanne Ogunah¹  | Reginah Wangui Ngari³ 

¹Department of Physical Sciences, University of Embu, Nairobi, Embu, Kenya | ²Department of Chemistry, Dedan Kimathi University of Technology, Nairobi, Nyeri, Kenya | ³Department of Chemistry, Multimedia University of Kenya, Nairobi, Ongata Rongai, Kenya

Correspondence: Nancy Mweni Paul (nancymuheni@gmail.com)

Received: 18 March 2025 | **Revised:** 26 December 2025 | **Accepted:** 12 February 2026

Academic Editor: Qian Fang

Keywords: compressive strength | ordinary Portland cement | scanning electron microscope (SEM) | supplementary cementitious materials (SCMs)

ABSTRACT

Rapid industrialization and urban growth have driven a rising demand for cement, yet ordinary Portland cement (OPC) production remains energy-intensive and a major source of CO₂ emissions. The partial substitution of OPC with supplementary cementitious materials (SCMs) offers a sustainable route to reduce environmental impact, production costs, and enhance performance. This study investigates the effects of replacing OPC with stone-cutting dust (SD), natural pozzolana (NP), and limestone (L) individually and in ternary blends on the compressive strength and microstructure of cement mortars. OPC was partially substituted with SD and NP at 10%–40% and with L at 5%–20%. Ternary blends containing SD, NP, and L replaced OPC at 25%–40%. Compressive strength was measured at 2, 7, 28, and 56 days, and microstructural analysis was performed at 28 days using scanning electron microscopy (SEM). Commercial OPC and Portland pozzolana cement (PPC) served as control samples. Results showed that strength development increased with curing age for all mixes. Optimal performance was recorded at lower substitution levels particularly 10%–20% NP, 5%–15% L, and ≤25% SD achieving 28-day strengths comparable to or exceeding OPC. High replacement levels (≥35%) reduced strength due to dilution of reactive clinker phases. Ternary blends demonstrated synergistic effects when reactive pozzolanic material and fine limestone were balanced, producing dense microstructures with refined pores and abundant calcium–silicate–hydrate (C–S–H) gel. SEM observations confirmed that improvements in compressive strength were associated with increased C–S–H formation, reduced calcium hydroxide (CH), and better particle packing in optimized mixes. These findings indicate that SD, NP, and L can be used effectively in partial substitution of OPC to produce environmentally friendly cement with satisfactory mechanical performance. Optimized blends can reduce OPC content by up to 25% without compromising strength, supporting sustainable construction practices while promoting the utilization of locally available industrial by-products. PPC was only used as a microstructural reference to compare hydration morphology with blended OPC systems, while OPC was utilized as the mechanical control for compressive strength evaluation.

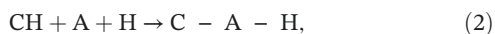
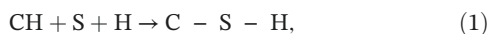
This is an open access article under the terms of the [Creative Commons Attribution](https://creativecommons.org/licenses/by/4.0/) License, which permits use, distribution and reproduction in any medium, provided the original work is properly cited.

Copyright © 2026 Nancy Mweni Paul et al. *Advances in Civil Engineering* published by John Wiley & Sons Ltd.

1 | Introduction

In recent years, various approaches have been initiated which includes studies of supplementary cementitious materials (SCMs) that can viably be utilized to partially substitute ordinary Portland cement (OPC), aiming to reduce production costs, environmental issues associated with greenhouse gas emissions while enhancing the physicochemical properties of cement mortars and concrete [1]. Natural pozzolana (NP), limestone, and stone-cutting dust (SD) are potential locally prepared cementitious materials that can be used to blend OPC. These materials are relatively cheaper than OPC which is major cement in constructions [2].

NP is an aluminous and siliceous containing material that reacts with calcium hydroxide (CH) from hydrating cement to produce a compound of cementitious properties [3]. The pozzolanic reaction for hydration can be represented as given in Equations (1) and (2) [4].



where S is silicates (SiO_2), A is aluminates (Al_2O_3), CH or $\text{Ca}(\text{OH})_2$ is lime, and H is water (H_2O). The use of pozzolanic materials is expected to improve the physicochemical properties of cement concrete and mortars. They include strength, durability, and workability of cement [5].

Limestone as a supplementary material produces a much denser particle packing and a greater particle distribution since it grinds finer [6]. The limestone's physical effects are linked to the increase in compressive strength of mortar and concrete due to the mineral powder's physical filler effect [7]. As a result, the concrete matrix microstructure is improved, the pore structure is refined and voids between the cement grains are filled, and thereby increasing the strength [8]. Limestone is rich in calcium carbonate (CaCO_3), which reacts with alumina and silica to form calcium (Ca) silicates and Ca aluminates in presence of water [9]. These compounds contribute to the durability and strength of cement, improving its long-term performance and its ability to resist cracking [10].

SD as a sustainable resource offers several potential benefits [11]. SD which is a by-product of quarrying operations can be effectively utilized rather than being disposed of as waste. This promotes sustainable resource management and reduces the environmental impact associated with stone dust disposal [12]. SD contains mineral compounds which include silica, alumina, and iron oxide [13]. These mineral compounds react with lime from hydrating cement to form additional cementitious materials enhancing the properties of cement mortars [14].

Effects of substituting OPC with NP, limestone, and SD based on its compressive strength and microstructure vis-à-vis commercially available Portland pozzolana cement (PPC) was investigated in this study. Comparing OPC blended with a mixture SD, NP, and limestone to commercially available PPC is essential for performance evaluation [15]. This comparison determines if the blended OPC meets or exceeds the performance standards and requirements expected of a pozzolanic cement [16]. The results were used to assess the viability of using a mixture of SD, NP, and limestone in terms of cost-effectiveness, environmental impact, or performance

in comparison to traditional materials and as a way of promoting waste reduction and resource efficiency.

This study investigates the effects of partially substituting OPC with SD, NP, and limestone (L), used individually and in ternary blends, on compressive strength development and microstructural characteristics of cement mortar. Commercial OPC was employed as the mechanical control for compressive strength evaluation, while commercially available PPC was included solely as a reference material for comparative microstructural analysis using scanning electron microscopy (SEM). The comparison with PPC was intended to provide context for hydration morphology and phase development rather than mechanical benchmarking. The study aims to identify optimal replacement levels that reduce OPC content while maintaining satisfactory mechanical performance and promoting sustainable utilization of locally available materials.

2 | Materials and Methods

2.1 | Materials, Sampling, and Characterization

OPC (42.5 N) and PPC (32.5 N) were purchased from appointed distributors within Athi River town, Kenya. ISO standard sand conforming to EN 196-1:2016 was sourced from Savannah Cement Ltd company, Kitengela, Kenya. Limestone (L) was sourced from Athi river mining company, Nairobi, Kenya. SD was sourced from Nguruga, Kajiado county, Kenya which lies between latitudes 1030' and 2 000' S. and longitudes 360 30' and 370 30' E, and at an altitude of 1710 m above sea level. NP was acquired from Nguruga, Kajiado County, Kenya. Distilled water was used in all activities in this study whenever water was being used.

OPC (42.5 N) and PPC (32.5 N) were used as control binders. OPC (42.5 N) and PPC (32.5 N) were used as control binders. Mechanical testing focused on OPC and blended mixes; PPC was not subjected to compressive strength testing and was used only for microstructural comparison. Their oxide compositions were obtained from manufacturer specifications. The chemical compositions of NP and L were determined using X-ray fluorescence (XRF) with a PANalytical Epsilon 3XLE spectrometer. For each test material, 0.900 g was weighed into an empty platinum crucible. A total of 9.000 g of lithium tetraborate was introduced into the sample as a flux and mixed for homogeneity. The obtained mixture was then put in a M4 gas fusion chamber for 17 min and fused to produce a glass bead. Before analyzing the glass beads in the XRF chamber, they were placed in a desiccator to cool [17]. For SD, the elemental composition of the raw powder was obtained using SEM coupled with energy dispersive X-ray spectroscopy (SEM-EDS). This provided a semiquantitative analysis of major oxides based on spot and area scans of representative particles.

Tables 1–3 present the oxide compositions of NP, SD, and L. The XRF analysis showed that NP contained a high proportion of silica ($\text{SiO}_2 = 48.90\%$) and alumina ($\text{Al}_2\text{O}_3 = 14.68\%$), along with Fe_2O_3 (7.24%), CaO (8.16%), and MgO (3.84%), confirming its pozzolanic character. The limestone exhibited significant MgO content, indicating a dolomitic character rather than a purely calcitic composition. This dolomitic nature suggests that limestone in this study primarily acts as a filler and nucleation agent and may influence carboaluminate formation during cement hydration. The elemental composition of SD, determined by SEM-EDS, showed a high CaO content of 52.13%, significant SiO_2 (22.48%), and lower levels of

TABLE 1 | Chemical composition of natural pozzolana.

Sample Id oxide	Natural pozzolana_Np1 (% mean ± Sd)	Sample Id oxide	Natural pozzolana_Np2 (% mean ± Sd)
Al ₂ O ₃	9.7591 ± 0.2923	MgO	0.4099 ± 0.3653
SiO ₂	64.6774 ± 0.4713	Al ₂ O ₃	8.6069 ± 0.2924
P ₂ O ₅	<LOD ± 0.014	SiO ₂	61.7015 ± 0.4845
SO ₂	<LOD ± 0.0179	P ₂ O ₅	<LOD ± 0.0155
TiO ₂	1.1273 ± 0.0974	SO ₂	<LOD ± 0.02
Cr ₂ O ₃	0.0185 ± 0.0133	TiO ₂	1.4401 ± 0.1119
MnO	0.6087 ± 0.0296	V ₂ O ₅	<LOD ± 0.0229
Fe ₂ O ₃	18.3946 ± 0.1428	Cr ₂ O ₃	0.0241 ± 0.0147
CoO	0.0407 ± 0.0273	MnO	0.6637 ± 0.0324
NiO	0.0603 ± 0.0109	Fe ₂ O ₃	21.0488 ± 0.1611
CuO	<LOD ± 0.0051	CoO	0.0438 ± 0.0303
ZnO	0.0811 ± 0.0055	NiO	0.066 ± 0.0123
As ₂ O ₃	<LOD ± 0.0465	CuO	<LOD ± 0.006
SeO ₂	<LOD ± 0.0039	ZnO	0.0901 ± 0.0062
SnO ₂	0.2109 ± 0.1657	As ₂ O ₃	<LOD ± 0.0516
PbO	<LOD ± 0.0628	SeO ₂	<LOD ± 0.0056
—	—	SnO ₂	0.2739 ± 0.1796
—	—	PbO	<LOD ± 0.0667

TABLE 2 | Chemical composition of limestone.

Sample ID oxide	Limestone_L2 (% mean ± SD)	Limestone_L1 (% mean ± SD)
MgO	39.6324 ± 3.1543	41.7272 ± 3.191
Al ₂ O ₃	8.4983 ± 1.1877	9.5901 ± 1.2321
SiO ₂	21.4716 ± 0.5938	19.6642 ± 0.5747
P ₂ O ₅	3.7989 ± 0.1340	3.8166 ± 0.1339
SO ₂	0.7135 ± 0.1000	0.7895 ± 0.1004
TiO ₂	<LOD ± 0.1340	<LOD ± 0.1225
V ₂ O ₅	<LOD ± 0.0580	<LOD ± 0.0500
Cr ₂ O ₃	<LOD ± 0.0381	0.0414 ± 0.0387
MnO	0.1066 ± 0.0364	0.1299 ± 0.0378
Fe ₂ O ₃	2.2756 ± 0.1187	2.3348 ± 0.1179
CoO	<LOD ± 0.0237	<LOD ± 0.0240
NiO	0.2832 ± 0.0324	0.2643 ± 0.0318
CuO	0.0262 ± 0.0147	0.0376 ± 0.0150
ZnO	<LOD ± 0.0110	<LOD ± 0.0109
As ₂ O ₃	<LOD ± 0.1812	<LOD ± 0.2263
SeO ₂	<LOD ± 0.0164	<LOD ± 0.0216
PbO	<LOD ± 0.3172	<LOD ± 0.3909

TABLE 3 | Elemental composition of stone-cutting dust (SD) raw powder determined by SEM–EDS, expressed as weight percentage (Wt%).

Element	Line type	Apparent concentration	k ratio	Wt%	Wt% sigma	Standard label	Factory standard
C	K series	0.54	0.00545	4.13	0.44	C Vit	Yes
O	K series	47.23	0.15893	47.36	0.28	SiO ₂	Yes
Na	K series	0.48	0.00203	0.53	0.04	Albite	Yes
Mg	K series	1.42	0.00941	1.86	0.05	MgO	Yes
Al	K series	9.55	0.06857	11.98	0.10	Al ₂ O ₃	Yes
Si	K series	16.29	0.12908	21.85	0.15	SiO ₂	Yes
P	K series	0.35	0.00194	0.36	0.04	GaP	Yes
K	K series	0.41	0.00351	0.51	0.04	KBr	Yes
Ca	K series	2.68	0.02393	3.84	0.07	Wollastonite	Yes
Ti	K series	5.06	0.05556	8.04	0.06	Ti	Yes
Fe	K series	4.78	0.04782	7.23	0.15	Fe	Yes
Total	—	—	—	100.00	—	—	—

Al₂O₃ (5.94%), Fe₂O₃ (2.84%), and MgO (1.98%), suggesting potential both as a filler and for limited pozzolanic contribution.

It should be noted that the SEM micrographs presented later in the results section depict hydrated paste samples at 28 days of curing, not unhydrated raw powders, and are used to illustrate microstructural development. No SEM images of unhydrated NP or L are included.

2.2 | Mix Formulations, Sample Preparation, and Optimization of the Ratios

The test materials, NP, limestone, and SD were ground using a laboratory ball mill to accomplish fine and consistent particle sizes suitable for cement blending. Sieve analysis was performed to confirm that the distribution of particle size fell within the required range and to ensure consistency across all samples. Each material was blended with OPC in specified proportions by weight, as outlined in the experimental design.

Each material was tested individually as a replacement for OPC, and mix codes were assigned for concise identification (e.g., NP10 = 10% NP, SD25 = 25% SD, L15 = 15% L). A summary of all mix formulations is presented in Table 4.

The optimization of replacement ratios in this study was informed by previous research that demonstrated the performance benefits of using SCMs in partial substitution of OPC. Ground samples of SD and NP were individually blended into OPC at replacement levels of 10%, 20%, 25%, 30%, 35%, and 40%, in line with studies which reported that pozzolanic and siliceous materials improve long-term strength when used within these ranges [18, 19]. Limestone was also partially substituted at 5%, 10%, 15%, and 20%, following the recommendations of Khatib et al. [20], who noted improved early strength and packing density at lower limestone dosages [21].

Additionally, ternary blends of NP, limestone, and SD were prepared and substituted into OPC at 25%, 30%, 35%, and 40%. These blend ratios were guided by findings from Elyasigorji et al. [22], who proved that combining reactive and inert materials in carefully

balanced proportions can yield synergistic effects in strength. The selected proportions aimed to explore a wide performance spectrum while ensuring that the combined replacement levels remained within acceptable limits for structural applications [23].

2.3 | Preparation of Mortar Prisms

According to the guidelines in KS EAS 148:1-2017, test cements were made using molds of measurements 40 mm × 40 mm × 160 mm. The water–cement ratio was 0.50, and the cement–sand ratio was 1:3 by mass (450 g cement, 225 g water, and 1350 g ISO standard sand). The control samples comprised of commercial OPC and commercial PPC. A total of 450 g of cement were weighed and added to 225 g distilled water in the bowl of the automatic programmable mortar mixer.

The bowl with its contents was then fixed on the automatic programmable mixer and allowed to start mixing at a low speed. After 30 s, 1350 g of standard sand prepared according to ISO 679:1989, EN 196–1 (2016) was gradually added into the bowl for the next 30 s. The machine was then programmed to run at maximum speed for the next 30 s and paused for 90 s. Using a plastic scoop, the mortar on the bowl's surface was scraped off and the entire mortar was scraped to one side of the bowl. After that, the mixer ran for 60 s at maximum speed.

The generated mortar was then transferred in 40 mm × 40 mm × 160 mm molds to make three mortar prisms at a go. The mortar was being filled into these steel molds in two stages, at first, they were half filled and compacted for 1 min with aid of a jolting machine after which the molds were fully filled and compacted again by a jolting machine for another 1 min. The mortar that had deep struck off during compacting and was on the mold's surface was removed by wiping it off.

The mold was then removed from the jolting machine and placed inside the humidity cabinet set at 20 ± 2°C temperature and humidity above 95% for 24 h after which it was removed and demoulded. The prisms were then cured in distilled water maintained at 25 ± 10°C temperature with the 40 mm × 40 mm side as the base

TABLE 4 | Mixture proportions of cements.

S/number	Stone-cutting dust (%)	Limestone (%)	Natural pozzolana (%)	OPC (%)	Naming
1	0	0	0	100	OPC
2	0	0	10	90	10% NP
3	0	0	20	80	20% NP
4	0	0	25	75	25% NP
5	0	0	30	70	30% NP
6	0	0	35	65	35% NP
7	0	0	40	60	40% NP
8	0	5	0	95	5% L
9	0	10	0	90	10% L
10	0	15	0	85	15% L
11	0	20	0	80	20%L
12	10	0	0	90	10% SD
13	20	0	0	80	20% SD
14	25	0	0	75	25% SD
15	30	0	0	70	30% SD
16	35	0	0	65	35% SD
17	40	0	0	60	40%SD
18	10	5	10	75	10% SD + 5% L + 10% NP (A)
19	15	5	5	75	15% SD + 5% L + 5% NP (B)
20	5	5	15	75	5% SD + 5% L + 15% NP (C)
21	5	10	15	70	5% SD + 10% L + 15% NP (D)
22	10	10	10	70	10% SD + 10% L + 10% NP (E)
23	15	10	5	70	15% SD + 10% L + 5% NP (F)
24	5	10	20	65	5% SD + 10% L + 20% NP (G)
25	10	10	15	65	10% SD + 10% L + 15% NP (H)
26	15	10	10	65	15% SD + 10% L + 10% NP (I)
27	20	10	5	65	20% SD + 10% L + 5% NP (J)
28	5	15	20	60	5% SD + 15% L + 20% NP (K)
29	10	15	15	60	10% SD + 15% L + 15% NP (L)
30	15	15	10	60	15% SD + 15% L + 10% NP (M)
31	20	15	5	60	20% SD + 15% L + 5% NP (N)

for 3, 7, 28, and 56 days. This procedure was repeated for all the cement categories and the control samples.

2.4 | Microstructure Determination After 28 Days of Curing

The 28th-day test samples were prepared for SEM as well as EDS analysis in accordance with Scrivener et al. [24], to identify the microstructure, morphology, as well as elemental content of cements. Hardened cement mortar specimens were impregnated using waterproof resin ERL-4206 to prevent cracking when analyzed using SEM. The SEM analysis was carried out on the cement

samples using a Zeiss Ultra Plus FEG-SEM equipped to work under high vacuum to preserve the integrity of the microstructure images. The SEM analysis facilitated observation of morphology, such as distribution of Ca-silicate-hydrate (C-S-H), ettringite, as well as unreacted particles. EDS was employed simultaneously together with SEM imaging to determine both qualitatively and quantitatively the elemental content of the cement matrix. The principle of operation of EDS lies on the emission of characteristic X-rays from atoms in a sample upon being excited by a focused beam of electrons. Detection of these produced X-rays by a silicon drift detector (SDD) enables one to identify as well as measure elements present in a sample. EDS gave precise chemical data regarding important

elements like silicon (Si), aluminum (Al), iron (Fe), Ca, and oxygen (O) in mixed cement. Such elements are important in evaluating hydration behavior, together with possible pozzolanic reactions. Data provided by EDS supplemented SEM observations by indicating the existence of cementitious phases, as well as filler particles. Hence, SEM–EDS analysis together provided a complete insight into microstructural evolution as well as chemical integration of SD, NP, and limestone in the OPC matrix at 28 days of hydration.

2.5 | Compressive Strength Determination

Compressive strength tests were carried out on mortar prisms measuring 40 mm × 40 mm × 160 mm, prepared in accordance with Kenya Standard KS EAS 148-1:2000. Each prism was cast, compacted, and cured in water at 20 ± 2°C until the testing age. Strength was assessed after 3, 7, 28, and 56 days of curing.

At each age, three prisms per mix were tested. Each prism was split to obtain two halves in line with EN 196-1, solely to prepare halves for compression; no flexural strength data were recorded or reported. Each half (40 mm × 40 mm × 80 mm) was then loaded in compression on a computer-controlled universal testing machine (UTM) with the fractured surface facing downward, at a constant rate of 2400 N/s, until failure. The compressive strength for a prism was taken as the average of its two halves. The reported value for each mix is the mean of three prisms.

Prisms were used instead of cubes to follow the adopted standard and to allow both operations on the same specimens, while reporting only compressive strength. The standard deviation of compressive strength results was within the typical range for EN 196-1 mortar testing, generally below 5%, indicating good repeatability of the measurements.

3 | Results and Discussion

3.1 | Microstructure Analysis After 28 Days of Curing

The microstructural analysis presented in this section focuses on OPC, PPC, limestone-based, and SD-based cement systems for which SEM images were obtained at 28 days of curing. SEM observations for NP-rich and ternary blended systems are inferred based on trends observed in these systems, supported by compressive strength results and relevant literature.

3.1.1 | OPC Paste Morphology After 28 Days of Curing

Figure 1 shows the OPC paste micrograph which was done using SEM after the 28th day of curing.

The SEM micrograph in Figure 1 reveals a dense microstructure, dominated by C–S–H structures marked with blue labels. These appear as fibrous, gel-like, or foil-like phases, confirming efficient hydration and contributing significantly to the mechanical strength and densification of the cement paste.

CH crystals, indicated by the green labels, are clearly visible as well-formed hexagonal plate-like structures. CH plays a role in maintaining an alkaline environment favorable for continued hydration [25]. However, it does not directly enhance strength and, if present

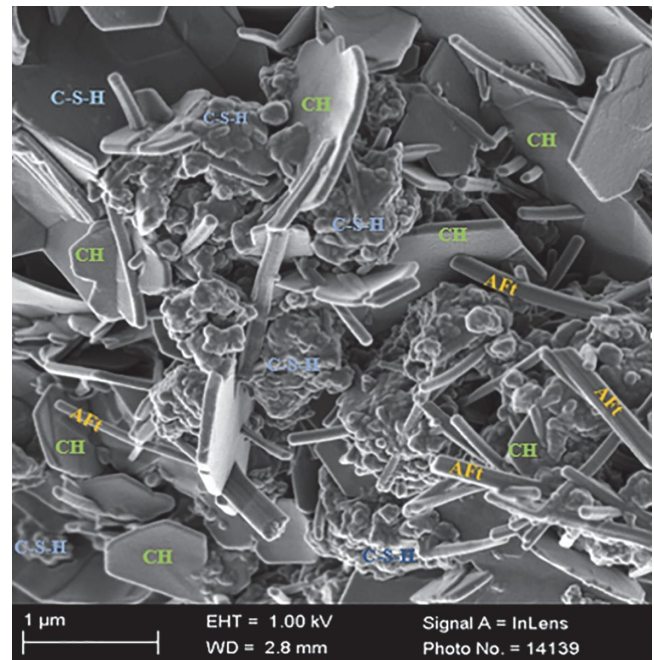


FIGURE 1 | OPC paste SEM micrograph after 28 days of curing. CH, calcium hydroxide; C–S–H, calcium–silicate–hydrate. Aft, ettringite.

in excessive amounts, can lower durability due to its relative solubility. The moderate amount observed suggests a healthy balance typical of well-cured OPC without significant pozzolanic interaction.

Ettringite (Aft) formations, highlighted by yellow labels, appear as fine needle-like or rod-shaped crystals. Their presence indicates active early-stage hydration reactions between aluminates and sulfates [26]. The moderate and well-distributed number of Aft points to effective gypsum contribution during cement setting without indications of excessive ettringite growth, which could otherwise risk delayed expansion or cracking.

These SEM observations are strongly supported by EDS elemental analysis, which showed high concentrations of Ca and Si, with minor Al contents. The chemical data confirm the dominance of C–S–H, along with appropriate levels of CH and Aft, consistent with expected hydration products of OPC.

The results are in agreement with previous findings reported by Ngari et al. [27], Musyoki et al. [28], and Mutitu et al. [29], reinforcing that traditional OPC hydration under water curing produces a robust and stable microstructure rich in C–S–H, moderate CH, and primary ettringite.

3.1.2 | PPC Morphology After 28 Days of Curing

Figure 2 shows the SEM image for PPC after undergoing curing for 28 days.

The SEM image in Figure 2 shows a microstructure dominated by a dense network of C–S–H, identifiable by the red labels. The C–S–H appears as fine, fibrous, and gel-like masses that fill most of the surface area. This dominant presence of C–S–H is attributed to the pozzolanic reaction: the active siliceous and aluminous materials in PPC react with the CH released during OPC hydration, forming additional C–S–H [30]. As a result, PPC microstructure exhibits

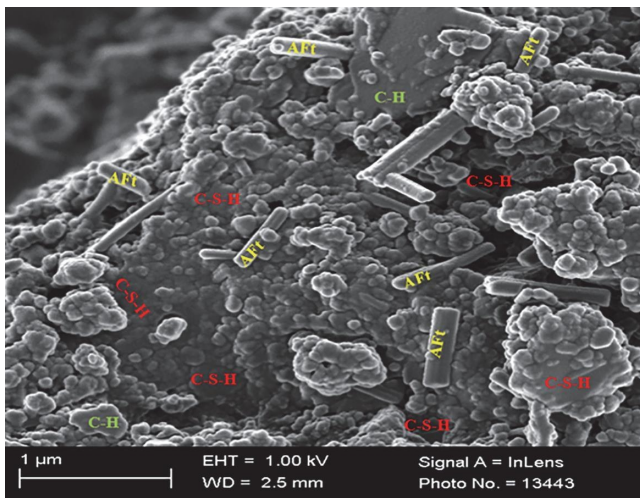


FIGURE 2 | PPC SEM micrographs after 28 days of curing. CH, calcium hydroxide; C-S-H, calcium-silicate-hydrate. Aft, ettringite.

higher quantities of C-S-H compared to plain OPC, enhancing strength and microstructural density.

The CH crystals, marked with green labels, appear in lower amounts and as scattered plate-like hexagonal crystals. The reduced presence of CH indicates an efficient pozzolanic reaction, consuming CH and producing more strength-giving C-S-H, thus improving the long-term durability of the paste.

Ettringite (Aft), distinguished by yellow/orange labels, is also visible as rod- or needle-like crystals dispersed throughout the matrix. Their presence suggests active reactions involving sulfate sources, not only from gypsum but also from the pozzolanic materials blended in PPC [31]. The well-formed Aft crystals contribute to early age strength and dimensional stability, although their controlled distribution suggests a low risk of future expansion or secondary ettringite formation [32].

The SEM observations are corroborated by the EDS elemental analysis, which confirmed elevated Si and Al contents alongside Ca, all of which support the abundant formation of C-S-H and Aft phases. These findings align with the microstructural characteristics expected from pozzolan-rich blended cements, as reported by Wang [33].

3.1.3 | Limestone Morphology After 28 Days of Curing

After 28 days of curing, the morphology of a limestone-based cement was examined using SEM, as shown in Figure 3.

The SEM micrograph in Figure 3 shows a microstructure where CaCO₃, indicated by the blue labels, is more prominently observed. This confirms the active contribution of limestone particles within the hydrated system [34]. The CaCO₃ mainly originates from the partial dissolution of the limestone and its involvement in secondary hydration processes [35].

CH, shown with red labels, is observed in relatively lower amounts compared to typical OPC systems. The reduction of CH is attributed to its reaction with the calcite (CaCO₃) from the limestone, which combines with tricalcium aluminate (C₃A) from the Portland clinker and CH to form Ca carboaluminate phases [36]. This reaction improves the durability and reduces free CH, stabilizing the microstructure [37].

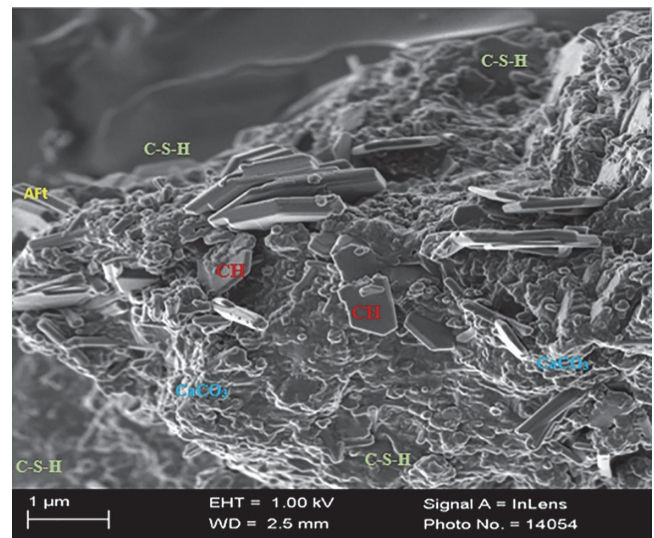


FIGURE 3 | Limestone-based SEM micrographs after 28 days of curing. CaCO₃, calcium carbonate; CH, calcium hydroxide; C-S-H, calcium-silicate-hydrate. Aft, ettringite.

The presence of C-S-H, identified with green labels, remains dominant, appearing as gel-like and foil structures. The limestone particles also act as nucleation sites, promoting early hydration of tricalcium silicate (C₃S) and dicalcium silicate (C₂S), thus leading to greater deposition of strength-giving C-S-H.

Ettringite (Aft), indicated by yellow labels, is present, but appears reduced compared to OPC pastes. This reduction is attributed to the limestone's ability to stabilize ettringite formation and limit secondary ettringite expansion, enhancing dimensional stability and microstructural compactness [38].

The SEM findings are in agreement with EDS elemental data, which confirms significant presence of Ca, Si, and carbon (C), reinforcing the visual identification of C-S-H, CH, CaCO₃, and Aft. This microstructural refinement due to limestone incorporation leads to a denser, more stable paste matrix after hydration [39].

3.1.4 | SD Morphology After 28 Days of Curing

Figure 4 shows the microstructure of stone-cutting based cement after 28 days of curing.

The SEM microstructure reveals a reduced presence of C-S-H, shown by the yellow labels, and CH, marked by the red labels, when compared to plain OPC pastes. This decline in C-S-H and CH content is attributed to the dilution effect caused by the partial replacement of cement with SD. The dilution interferes with the normal hydration process by reducing the quantity of reactive clinker phases, thereby decreasing the formation of C-S-H gel and CH [40].

The presence of CaCO₃, labeled in green, is also noted. This can be explained by the deliberate addition of 10% limestone during the mix design, as well as the possible inherent carbonate content in the SD itself [41]. The occurrence of CaCO₃ points to both physical filler effects and potential chemical interactions that could slightly contribute to early nucleation sites for C-S-H formation, albeit at a reduced scale compared to pure OPC [30].

Ettringite (Aft) formations, indicated by the light blue labels, are still visible as fine needle-like structures. Their presence suggests

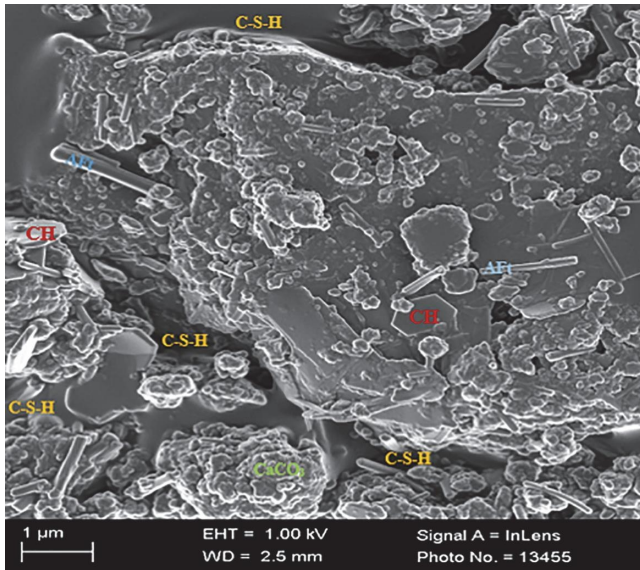


FIGURE 4 | Stone-cutting based SEM micrographs after 28 days of curing. CaCO_3 : Calcium carbonate; CH, calcium hydroxide; C-S-H, calcium-silicate-hydrate. AFt, ettringite.

that the basic sulfate-aluminate reactions proceed even in the modified matrix, although the extent of AFt development is relatively modest compared to OPC systems.

Overall, the SEM observations align with the EDS results, which indicated lower Si and Ca peaks relative to OPC, confirming the interference of hydration due to the SD addition. These findings demonstrate the impact of using stone-cutting waste materials on the hydration behavior and microstructure of blended cement systems [42].

3.2 | Compressive Strength

3.2.1 | OPC Paste

Figure 5 below shows the compressive strength development for OPC at the 3rd, 7th, 28th, and 56th days of curing.

Figure 5 presents the development in compressive strength in OPC with varied curing ages: 3, 7, 28, and 56 days. The evidence depicts an increasing trend with progress in days, commencing from

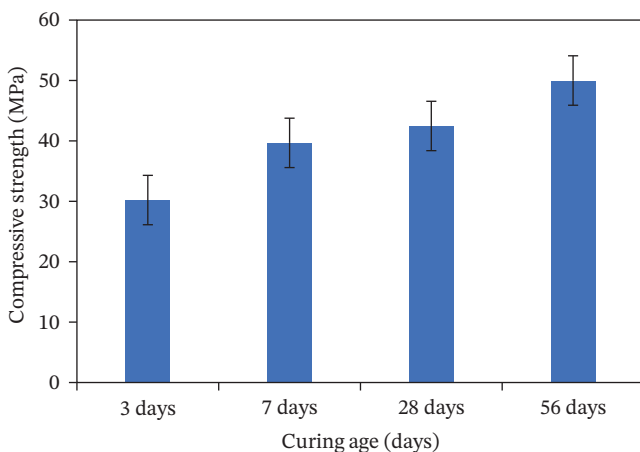


FIGURE 5 | Compressive strength development for OPC paste.

30 MPa on the 3rd day and reaching about 39 MPa on the 7th day and around 43 MPa on the 28th day. On the 56th day, the compressive strength continues to ramp up to 50 MPa, indicating ongoing hydration in clinker phases, chiefly C_3S . The behavior is characteristic of OPC in general, with greater early strength being developed in the initial week and subsequent curing enhancing further the refinement in the microstructure through ongoing C-S-H gel growth [43]. Evidence of steady progress in strength affirms successful hydration and sustains the microstructural findings in SEM observation with dense networks of products of hydration being visible. The evidence is used to provide comparative exposure to the blended cement prepared in this study to judge the performance of alternative materials like limestone, NP powder, and SD to replace some OPC [44]. Strength results showed low scatter across replicate specimens, indicating good repeatability of the compressive strength measurements.

3.2.2 | OPC Substituted With NP

Figure 6 shows compressive strength development for OPC substituted with NP at the 3rd, 7th, 28th, and 56th days of curing.

Figure 6 indicates the development in compressive strength in cement mixes with OPC partially replaced with NP with substitution levels of 10%, 20%, 25%, 30%, 35%, and 40%, and monitored at 3, 7, 28, and 56 days of curing. At 3 days, all samples with pozzolana substitution are lower in strength than pure OPC with 10% substitution achieving approximately 28 MPa and 40% substitution recording the lowest at approximately 19 MPa. The initial dip reflects the poorer early reactivity of pozzolana compared to OPC. At 7 days, there are increases in strength in all the mixes with 10% substitution achieving nearly 38 MPa, indicating the beginning of early pozzolanic reaction. At 28 days, there are further increases with 10% and 20% substitution achieving near or above 40 MPa and clearly showing high long-term reactivity of the pozzolanic material. At 56 days, 10% substitution records more than 48 MPa and catches up slightly with pure OPC. While the greater levels of substitution (30%–40%) remain behind in absolute value, the gradual increases with time continue to show; these findings validate that lower substitution levels (especially 10%–20%) tip the scales towards early and long-term strength with equal effectiveness and thus are ideal to enhance sustainability without sacrificing mechanical performance by any significant margin.

From Figure 6, the compressive strength was found to increase with increase in the curing age which can be credited to the role of the silicate and aluminate phases [45]. These phases reacted with the CH produced during the hydration of the cement to form cementitious products [46]. Nonetheless, it was observed that as the mass percentage of NP in OPC replacement was being increased, the compressive strength was reducing at all days. These outcomes were consistent to what Hussein et al. [47] found. The decrease in compressive strength with increasing substitution was because SiO_2 from NP, which has comparatively lower reactivity, partially replaced C_3S and C_2S phases [48].

3.2.3 | OPC Substituted With Limestone

Figure 7 shows compressive strength development for OPC substituted with limestone at the 3rd, 7th, 28th, and 56th days of curing.

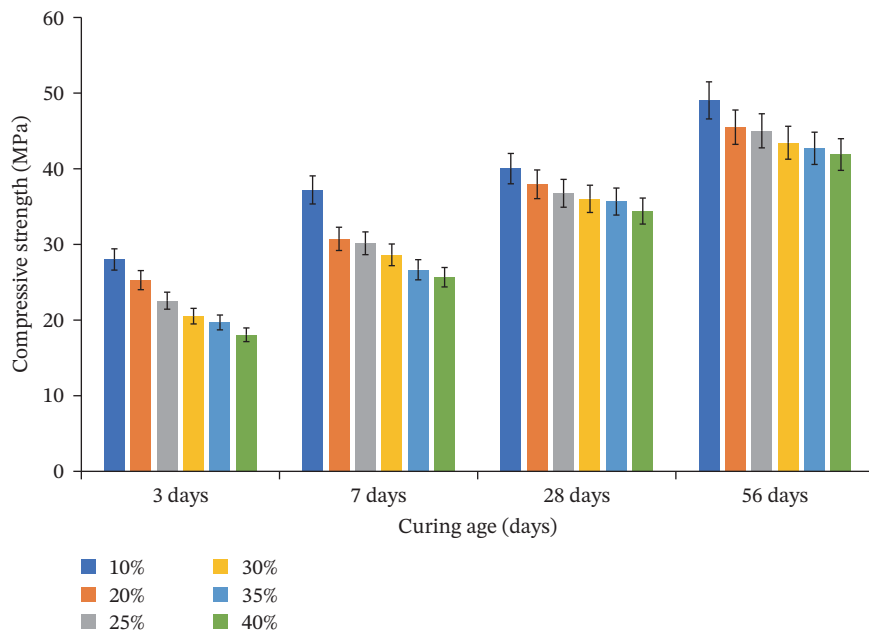


FIGURE 6 | Compressive strength of OPC blended with natural pozzolana.

As observed in Figure 7, there was an increase in compressive strength across the curing age. This can be attributed to Ca carboaluminates compounds formed when calcite (CaCO_3) from limestone reacts with C_3A of Portland clinker in presence of CH from hydrating cement, which promote strength development. Also, the limestone particles provide nucleation sites for C_3S and C_2S hydration leading to the deposit of C–S–Hs (filler effect) which are responsible for compressive strength development [49].

Compressive strength directly decreased as the amount of limestone substituted increased. When limestone is substituted in excess of the optimum amount, only fill the voids between the particles, increasing the material's compactness and, thus, its mechanical strength. Once the voids are completely filled, the additional filler

material begins to replace the primary aggregate grain, reducing the mechanical strength of the composite [50]. Additionally, the decrease in compressive strength with increase in limestone content can be as a result of the dilution effect which indicate that relatively inert limestone is replacing the reactive clinker phases in cement [51].

3.2.4 | OPC Substituted With SD

Figure 8 shows the compressive strength development for OPC substituted with SD at the 3rd, 7th, 28th, and 56th days of curing.

Figure 8 presents the compressive strength development of cement mixes where OPC was partially replaced with 10% to 40% SD, tested

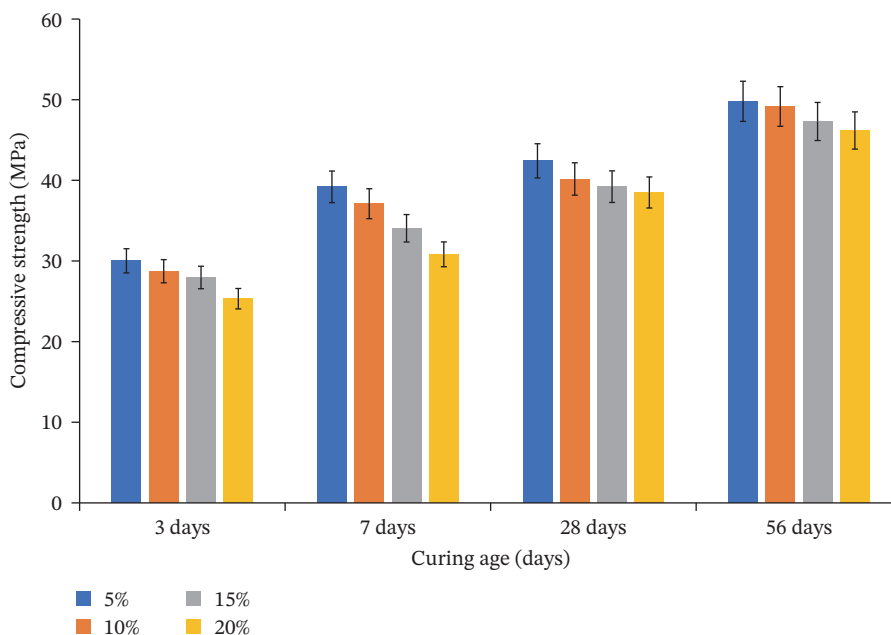


FIGURE 7 | Compressive strength of OPC blended with limestone.

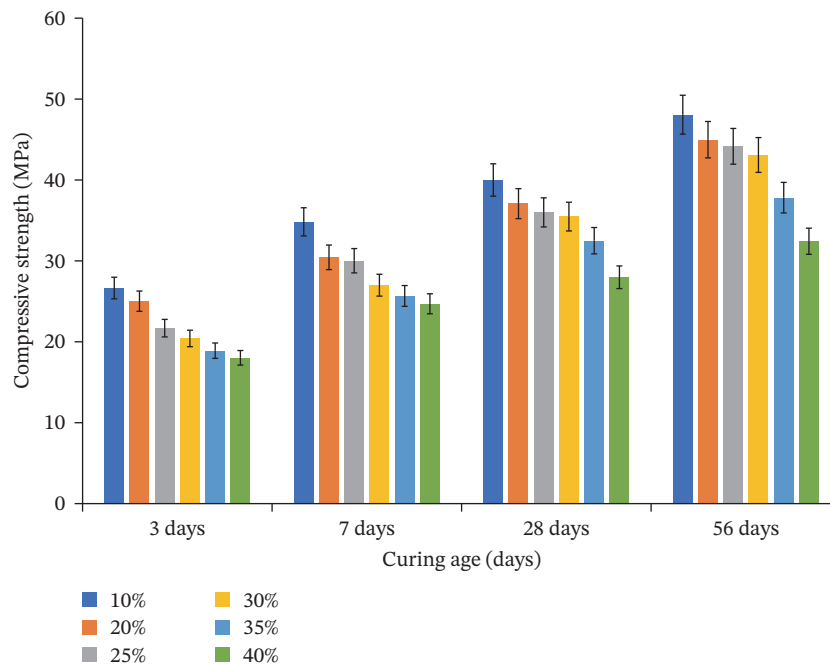


FIGURE 8 | Compressive strength of OPC blended with stone-cutting dust.

at 3, 7, 28, and 56 days of curing. At 3 days, compressive strength was highest in the 10% blend at approximately 27 MPa, while the 40% blend recorded the lowest at about 18 MPa, indicating a dilution effect at higher substitution levels during early hydration. By the 7th day, strength improved across all blends, with the 10% and 20% substitutions reaching 35 and 31 MPa, respectively. At 28 days, the 10% blend achieved around 40 MPa, while 25% and 30% blends followed closely, showing that moderate substitution levels retain strength development comparable to lower blends. By 56 days, the 10% mix peaked at nearly 48 MPa, followed by 20% and 25% blends above 44 MPa, while the 40% blend lagged at approximately 33 MPa. These results confirm that SD is most effective when used at substitution levels up to 25%, where it contributes beneficially to long-term strength without compromising the cement's structural integrity.

As observed in Figure 8, as the curing age increased, the compressive strength increased as well. The compressive strength is enhanced by the pozzolanic qualities of SD, which promote chemical reactions that result in the development of C–S–Hs [52]. Nonetheless, the compressive strength decreased as the amount of SD substituted increased. The decrease in C–S–H was most likely due to the dilution effect brought on by the addition of SD interfering with the hydration process [53].

3.2.5 | OPC Substituted With a Mixture of SD, Limestone, and NP

Figure 9 shows compressive strength development for OPC substituted with a mixture of SD, limestone, and NP at the 3rd, 7th, 28th, and 56th days of curing.

Substituting OPC with a mixture of SD, limestone (L), and NP while optimizing the ratios, the mixtures in Figure 9 with lower NP and SD content yielded higher compressive strength values. In contrast, mixtures which contained higher proportions of SD and NP,

demonstrated lower compressive strength values which can be attributed to the SiO₂ from pozzolanic materials, which has comparatively lower reactivity, partially replacing C₃S and C₂S phases that hydrate in presence of water to form C–S–H responsible for strength development [54]. Limestone, an inert filler, can improve particle packing and give hydration products places to nucleate, resulting in the deposit of C–S–H, which is what provides a material with its strength [55]. The observed strength enhancement suggests synergistic interactions among SD, limestone, and NP, which are consistent with microstructural trends reported in the literature for similar blended cement systems. For clarity, selected numerical comparisons are highlighted. At 56 days of curing, the NP10 mix achieved approximately 48 MPa compared to about 50 MPa for the OPC control, indicating closely comparable long-term strength. Similarly, the best-performing ternary blend reached approximately 45 MPa at 28 days, which is within about 10% of the OPC strength at the same curing age. These results confirm that optimized replacement levels can maintain mechanical performance while reducing OPC content.

4 | Conclusion

This study evaluated the effects of partially substituting OPC with SD, NP, and limestone (L), both individually and in ternary blends, on the compressive strength and microstructure of mortar. Replacement levels ranged from 5% to 40%, with commercial OPC and PPC serving as controls.

Results showed that compressive strength for all mixes increased with curing age, consistent with ongoing hydration and microstructural refinement. Optimized blends achieved 28–56 day compressive strengths within approximately 5%–10% of the OPC control. Optimal performance was achieved at lower substitution levels particularly 10%–20% NP, 5%–15% L, and ≤25% SD, where 28 and 56-day strengths were comparable to, or exceeded, OPC

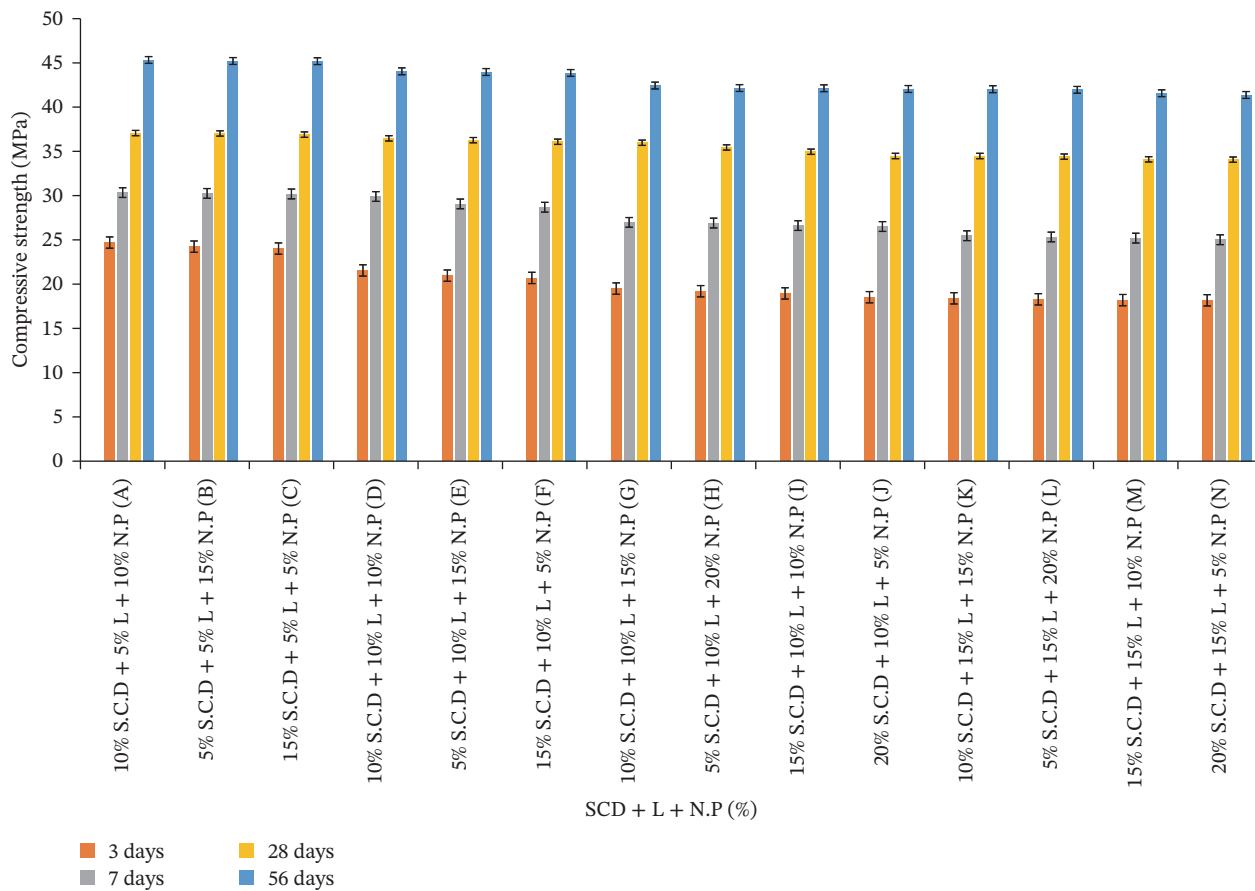


FIGURE 9 | Compressive strength of OPC blended with stone-cutting dust, limestone, and natural pozzolana.

controls. At higher replacement levels ($\geq 35\%$), dilution of reactive clinker phases led to strength reductions.

Microstructural analysis using SEM–EDS revealed that optimized blends exhibited dense and well-packed matrices with abundant C–S–H gel, reduced CH, and improved particle packing. Ternary blends demonstrated synergistic effects when reactive pozzolanic materials were balanced with fine limestone filler, enhancing both strength and microstructural compactness. The improved performance of optimized ternary blends indicates synergistic interactions that are consistent with microstructural behavior reported in previous studies on blended cement systems.

These findings indicate that locally available industrial by-products SD, NP, and L can effectively replace up to 25% of OPC in mortar production without compromising structural performance. Such substitutions offer environmental benefits through reduced clinker content and CO₂ emissions, lower production costs, and sustainable utilization of waste materials.

5 | Recommendations

1. Optimal replacement levels:

For structural applications, it is recommended to limit OPC substitution to $\leq 25\%$ for SD, 10%–20% for NP, and 5%–15% for L. These

levels maximize performance while maintaining cost-effectiveness and sustainability.

2. Ternary blend utilization:

Blends combining SD, NP, and L in balanced proportions should be prioritized for projects aiming for both environmental sustainability and improved durability, as they deliver synergistic strength and microstructural benefits.

3. Standardization and field trials:

Further field-scale validation is advised to confirm laboratory findings under real construction conditions. Standard mix codes and consistent proportioning guidelines should be developed for industry adoption.

4. Durability testing:

While compressive strength was the main focus of this study, future research should include long-term durability assessments such as sulfate resistance, chloride permeability, carbonation depth, and freeze–thaw performance to establish comprehensive performance profiles.

5. Policy and industry adoption:

Policymakers and construction stakeholders should encourage the use of industrial by-products as SCMs through updated building

codes, incentives, and awareness campaigns, supporting the shift toward greener cement production.

Author Contributions

Nancy Mweni Paul was responsible for the conceptualization, methodology, and the preparation of the original draft. Supervision of the research and the subsequent review and editing of the manuscript were conducted by Jackson Wachira Muthengia, Genson Murithi, and Joanne Ogunah. Additionally, Esther Wanja Nthiga and Reginah Wangui Ngari contributed through validation and data curation.

Funding

No funding was received for this manuscript.

Conflicts of Interest

The authors declare no conflicts of interest.

Data Availability Statement

The data that support the findings of this study are available upon request from the corresponding author. The data are not publicly available due to privacy or ethical restrictions.

References

1. A. A. Jhatial, I. Nováková, and E. Gjerløw, "A Review on Emerging Cementitious Materials, Reactivity Evaluation and Treatment Methods," *Buildings* 13, no. 2 (2023): 526.
2. J. M. Marangu, J. Karanja, and J. M. Wachira, "Review of Carbonation Resistance in Hydrated Cement Based Materials," *Journal of Chemistry* 2019, no. 1 (2019): 8489671.
3. S. Mousavinezhad, J. M. Garcia, W. K. Toledo, and C. M. Newton, "A Locally Available Natural Pozzolan as a Supplementary Cementitious Material in Portland Cement Concrete," *Buildings* 13, no. 9 (2023): 2364.
4. S. Velázquez, J. Monzó, M. V. Borrachero, L. Soriano, and J. Payá, "Evaluation of the Pozzolanic Activity of Spent FCC Catalyst/Fly Ash Mixtures in Portland Cement Pastes," *Thermochimica Acta* 632 (2016): 29–36.
5. O. Nassiri, I. Mahboub, M. Ibnoussina, et al., "Physico-Mechanical, Structural, and Mineralogical Analysis of Composite Concrete Incorporating Hydraulic Lime and Pozzolan," *Construction and Building Materials* 437 (2024): 136804.
6. K. Celik, C. Meral, A. Petek Gursel, P. K. Mehta, A. Horvath, and P. J. M. Monteiro, "Mechanical Properties, Durability, and Life-Cycle Assessment of Self-Consolidating Concrete Mixtures Made With Blended Portland Cements Containing Fly Ash and Limestone Powder," *Cement and Concrete Composites* 56 (2015): 59–72.
7. F. Lollini, E. Redaelli, and L. Bertolini, "Effects of Portland Cement Replacement With Limestone on the Properties of Hardened Concrete," *Cement and Concrete Composites* 46 (2014): 32–40.
8. M. Dobiszewska, O. Bagcal, A. Beycioğlu, et al., "Utilization of Rock Dust as Cement Replacement in Cement Composites: An Alternative Approach to Sustainable Mortar and Concrete Productions," *Journal of Building Engineering* 69 (2023): 106180.
9. N. Rakhimova, "Calcium and/or Magnesium Carbonate and Carbonate-Bearing Rocks in the Development of Alkali-Activated Cements – A Review," *Construction and Building Materials* 325 (2022): 126742.
10. R. Gettu, M. Santhanam, R. Pillai, and Y. Dhandapani, "Recent Research on Limestone Calcined Clay Cement (LC3) at IIT Madras Recent Research on Limestone Calcined Clay," (2018).

11. P. I. Modi and R. K. Gajjar, "Critical Review on Substitution of Natural Ingredients With the Dimensional Stone Cutting Waste in Making of Building Products," *ITEGAM- Journal of Engineering and Technology for Industrial Applications (ITEGAM-JETIA)* 10, no. 45 (2024).
12. J. Shao, J. Gao, Y. Zhao, and X. Chen, "Study on the Pozzolanic Reaction of Clay Brick Powder in Blended Cement Pastes," *Construction and Building Materials* 213 (2019): 209–215.
13. J. M. Terrones-Saeta, J. Suárez-Macías, F. A. Corpas-Iglesias, V. Korobiichuk, and V. Shamrai, "Development of Ceramic Materials for the Manufacture of Bricks With Stone Cutting Sludge From Granite," *Minerals* 10, no. 7 (2020): 621.
14. A. K. Singh, V. Srivastava, and V. C. Agarwal, "Stone Dust in Concrete: Effect on Compressive Strength," *International Journal of Engineering and Technical Research (IJETR)* 3, no. 8 (2015): 115–118.
15. P. Murthi, V. Lavanya, A. Bahrami, and K. Poongodi, "Performance Evaluation of Polypropylene Fiber-Reinforced Pavement Quality Concrete Made With Waste Granite Powder," *Buildings* 13, no. 5 (2023): 1294.
16. M. A. Al-Shugaa, A. Al-Fakih, W. Al-Awsh, and M. A. Al-Osta, "Pozzolanic Performance and Characteristic Analysis of Binary Blended Cement Incorporating Ceramic Polishing Sludge," *Journal of Materials Research and Technology* 29 (2024): 3711–3725.
17. O. M. Munyao, J. Karanja, J. M. Wachira, D. K. Mutitu, and R. Mwirichia, "Influence of *Starkeya novella* on Mechanical and Microstructural Properties of Cement Mortars," *Journal of Chemistry* 2020, no. 1 (2020): 8212396.
18. J. M. Marangu, A. O. Nyabuto, T. Pfeiffer, S. Kruschwitz, C. Völker, and W. Schmidt, "Sustainability Potentials of the Precast Industry in Kenya," in *The 1st International Conference on Net-Zero Built Environment*, eds. M. Kioumarsis and B. Shafei, (Springer Nature Switzerland, 2025): 1699–1710.
19. M. Antunes, R. L. Santos, J. Pereira, P. Rocha, R. B. Horta, and R. Colaço, "Alternative Clinker Technologies for Reducing Carbon Emissions in Cement Industry: A Critical Review," *Materials* 15, no. 1 (2022): 209.
20. J. M. Khatib, R. Ramadan, H. Ghanem, A. Elkordi, and M. Sonebi, "Effect of Limestone Fines as a Partial Replacement of Cement on the Chemical, Autogenous, Drying Shrinkage and Expansion of Mortars," *Materials Today: Proceedings* 58 (2022): 1199–1204.
21. D. P. Bentz, C. F. Ferraris, S. Z. Jones, D. Lootens, and F. Zunino, "Limestone and Silica Powder Replacements for Cement: Early-Age Performance," *Cement and Concrete Composites* 78 (2017): 43–56.
22. F. Elyasigorji, F. Farajiani, M. Hajipour Manjili, et al., "Comprehensive Review of Direct and Indirect Pozzolanic Reactivity Testing Methods," *Buildings* 13, no. 11 (2023): 2789.
23. J. Liu and J. Liu, "Experimental Investigation of the Effect of Ammonia Substitution Ratio on an Ammonia-Diesel Dual-Fuel Engine Performance," *Journal of Cleaner Production* 434 (2024): 140274.
24. K. L. Scrivener, V. M. John, and E. M. Gartner, "Eco-Efficient Cements: Potential Economically Viable Solutions for a Low-CO2 Cement-Based Materials Industry," *Cement and Concrete Research* 114 (2018): 2–26.
25. X. Chen, Q. Wang, Y. Ding, Q. Wu, Y. Chen, and Y. Liu, "Influence Mechanism of Alkaline Environment on the Hydration of Hemihydrate Phosphogypsum: A Comparative Study of Various Alkali," *Construction and Building Materials* 353 (2022): 129070.
26. S. Zhang, Z. Wu, J. Chen, R. Xu, M. Wang, and W. Ni, "Study on the Hydration Reaction of Typical Clay Minerals Under Alkali and Sulfate Compound Activation," *Gels* 8, no. 9 (2022): 564.
27. R. W. Ngari, J. K. Thiong'o, J. M. Wachira, G. Muriithi, and D. K. Mutitu, "Bioremediation of Mortar Made From Ordinary Portland

- Cement Degraded by *Thiobacillus thioeparus* Using *Bacillus flexus*,” *Heliyon* 7, no. 6 (2021): e07215.
28. D. M. Musyoki, J. W. Muthengia, J. Ogunah, et al., “Effect of Immobilizing *Bacillus megaterium* on the Compressive Strength and Water Absorption of Mortar,” *Journal of Chemistry* 2022 (2022): 1–12: 7752812.
29. K. D. Mutitu, M. O. Munyao, M. J. Wachira, R. Mwirichia, K. J. Thiong’o, and M. J. Marangu, “Effects of Biocementation on Some Properties of Cement-Based Materials Incorporating *Bacillus* Species Bacteria – a Review,” *Journal of Sustainable Cement-Based Materials* 8, no. 5 (2019): 309–325.
30. F. Wang, X. Kong, L. Jiang, and D. Wang, “The Acceleration Mechanism of Nano-C-S-H Particles on OPC Hydration,” *Construction and Building Materials* 249 (2020): 118734.
31. F. Zunino and K. Scrivener, “Insights on the Role of Alumina Content and the Filler Effect on the Sulfate Requirement of PC and Blended Cements,” *Cement and Concrete Research* 160 (2022): 106929.
32. M. J. Garba, C. Yu, J. Liu, et al., “Enhancing Long-Term Strength of Liquid-Accelerated Shotcrete: Effect of Nano-Silica and Synthesized Nano-Crystalline C-S-H Seeds,” *Construction and Building Materials* 459 (2025): 139798.
33. J. Wang, Z. Hu, Y. Chen, et al., “Effect of Ca/Si and Al/Si on Micromechanical Properties of C(-A)-S-H,” *Cement and Concrete Research* 157 (2022): 106811.
34. C. Li, X. Qian, Y. Tao, Y. Qin, C. Hu, and F. Wang, “In-Situ Active Interface Cementation via Nano-Engineered Partially Calcined Limestone Aggregates,” *Construction and Building Materials* 491 (2025): 142756.
35. R. Hay, B. Peng, and K. Celik, “Filler Effects of CaCO₃ Polymorphs Derived From Limestone and Seashell on Hydration and Carbonation of Reactive Magnesium Oxide (MgO) Cement (RMC),” *Cement and Concrete Research* 164 (2023): 107040.
36. D. Kong, T. Wang, J. Zhang, T. Li, and T. Liu, “Improvement of Strength and Microstructure of Low-Carbon Cementitious Materials With High Volume of Calcined Coal Gangue,” *Construction and Building Materials* 444 (2024): 137916.
37. Z. Liu, C. Deng, C. Yu, J. Ding, and H. Zhu, “Improving the Anti-Oxidation and Water Wettability of Graphite Through the Design of Coating Structure for the Preparation of Al₂O₃-SiC-C Castables,” *Ceramics International* 49, no. 17 (2023): 29104–29113.
38. I. Kharchenco, V. Alekseev, and O. Kalinina, “Effect of Ettringite Morphology on the Properties of Expanding Cement Systems,” in *2nd Symposium on Openfoam R in Wind Energy*, 110, (EDP Sciences, 2019): 01037.
39. C. Li and L. Jiang, “Utilization of Limestone Powder as an Activator for Early-Age Strength Improvement of Slag Concrete,” *Construction and Building Materials* 253 (2020): 119257.
40. D. Gastaldi, F. Bertola, S. Irico, G. Paul, and F. Canonico, “Hydration Behavior of Cements With Reduced Clinker Factor in Mixture With Sulfoaluminate Binder,” *Cement and Concrete Research* 139 (2021): 106261.
41. C. A. A. Rocha, G. C. Cordeiro, and R. D. Toledo Filho, “Influence of Stone Cutting Waste and Ground Waste Clay Brick on the Hydration and Packing Density of Cement Pastes,” *Revista IBRACON de Estruturas e Materiais* 6, no. 4 (2013): 661–680.
42. M. Salehi, M. Bayat, M. Saadat, and M. Nasri, “Experimental Study on Mechanical Properties of Cement-Stabilized Soil Blended With Crushed Stone Waste,” *KSCE Journal of Civil Engineering* 25, no. 6 (2021): 1974–1984.
43. Z. Long, G. Long, Z. Tang, et al., “Hydration, Strength, and Microstructure Evolution of Portland Cement-Calcium Sulphoaluminate Cement-CSH Seeds Ultra-Early Strength Cementitious System,” *Construction and Building Materials* 430 (2024): 136492.
44. M. Ahmadi, E. Abdollahzadeh, M. Kashfi, B. Khataei, and M. Razavi, “Life Cycle Assessment and Performance Evaluation of Self-Compacting Concrete Incorporating Waste Marble Powder and Aggregates,” *Materials* 18, no. 13 (2025): 2982.
45. A. Gulec, “Investigation of the Effect of Different Curing Conditions on the Mechanical Performance of Calcium Aluminate Cement Concrete at Elevated Temperatures,” *Construction and Building Materials* 409 (2023): 133920.
46. A. A. Hoyos-Montilla, J. I. Tobón, and F. Puertas, “Role of Calcium Hydroxide in the Alkaline Activation of Coal Fly Ash,” *Cement and Concrete Composites* 137 (2023): 104925.
47. K. M. Hussein, E. H. Bouchra, M. S. E. Youbi, and E. Ahmed, “Development and Study of Physical, Chemical and Mechanical Properties of a New Formulation of Cement of a Varying Percentage of Natural Pozzolan,” (2017).
48. K. Mwangi Wanjiku, J. W. Muthengia, J. Ogunah, et al., “Effects of *Lysinibacillus Sphaericus* on Physicomechanical and Chemical Performance of OPC Blended With Natural Tuff and Pulverized Fly Ash,” *Advances in Materials Science and Engineering* 2022 (2022): 1–15: 3387928.
49. G. D. Moon, S. Oh, S. H. Jung, and Y. C. Choi, “Effects of the Fineness of Limestone Powder and Cement on the Hydration and Strength Development of PLC Concrete,” *Construction and Building Materials* 135 (2017): 129–136.
50. M. El-Moussaoui, R. K. Dhir, and P. C. Hewlett, “Concrete Strength Development and Sustainability: The Limestone Constituent Cement Effect,” *Magazine of Concrete Research* 71, no. 21 (2019): 1097–1112.
51. P. Thongsanitgarn, W. Wongkeo, S. Sinthupinyo, and A. Chaipanich, “Effect of Limestone Powders on Compressive Strength and Setting Time of Portland-Limestone Cement Pastes,” *Advanced Materials Research* 343-344 (2011): 322–326.
52. S. Yagüe, C. González Gaya, V. Rosales Prieto, and A. Sánchez Lite, “Sustainable Ecocements: Chemical and Morphological Analysis of Granite Sawdust Waste as Pozzolan Material,” *Materials* 13, no. 21 (2020): 4941.
53. A. B. Passos, L. Onghero, P. R. de Matos, et al., “Assessment of the Chemical Reactivity of Brazilian Stone Cutting Plant Waste Into Cementitious Matrices,” *Sustainability* 14, no. 24 (2022): 16925.
54. D. Zhao, “Microstructure and Hydration of Cement-Based Materials Incorporating Calcined Clay and Calcium-Silicate-Hydrate (C-S-H) Seed,” (2020).
55. Y.-J. Kim, R. V. Leeuwen, B.-Y. Cho, V. Sriraman, and A. Torres, “Evaluation of the Efficiency of Limestone Powder in Concrete and the Effects on the Environment,” *Sustainability* 10, no. 2 (2018): 550.